24

Relationships between Large-Scale Coherent Motions and Bursting Events in a Turbulent Boundary Layer

Yasuhiko Sakai, Kouji Nagata and Hiroki Suzuki
Nagoya University
Japan

1. Introduction

A turbulent boundary layer (TBL) over a flat rigid surface can be seen in many industrial and environmental flows. Therefore, for the prediction and control of turbulence and design of better industrial apparatus, it is of great importance to elucidate the spatiotemporal structure of the TBL. In TBLs, it is well known that coherent motions associated with the bursting events exist near the wall. In the outer turbulent/nonturbulent (potential) interface of the TBL, large-scale coherent motions exist, which have the size of order of the boundary-layer thickness. The latter structures are called `bulge' and `valley' and are unsteady in space and time (Robinson 1991). Therefore, it is of importance to clarify the spatiotemporal structures of these coherent motions in order to elucidate the structure of the TBL. However, it is difficult to study the entire structure of the TBL by a single-point measurement using an I- or X-type hot-wire probe. In addition, previous studies (Ichijo & Kobashi 1982, Kobashi et al. 1984, Thomas & Bull 1983) have suggested that these coherent motions are closely associated with wall static pressure fluctuations. Therefore, the simultaneous measurement of multipoint instantaneous velocities and wall static pressure fluctuations is appropriate for clarifying the spatiotemporal structure of the TBL.

In this chapter, we will show the experimental results on the relationships between the bursting events occurring near the wall and the large-scale bulge and valley structures in the outer turbulent/nonturbulent interface of the TBL, and the spatiotemporal structures of the coherent motions in a zero-pressure-gradient TBL. With regard to the experiments, multipoint instantaneous streamwise velocities and instantaneous wall static pressures are simultaneously measured using a combination of a rake consisting of 23 I-type hot-wire probes, which covers the entire TBL, and a microphone pressure sensor. The velocity signals are analysed by the KL (Karhunen-Loéve) expansion (also known as the proper orthogonal decomposition (POD) method). The flow field is reconstructed by using either lower- or higher-order modes to investigate the coherent motions in the TBL. The bursting events are detected by applying the VITA (Variable Interval Time Average) technique to the instantaneous velocity signals in the original flow. The large-scale bulge and valley structures are detected by using the newly proposed conditional sampling method, which is applied to both the original flow and the reconstructed flow by using the KL expansion. Further, to show the future research direction, the experimental data on the statistical

properties of TBL affected by the disturbances in the outer mainstream are demonstrated. The disturbances are generated using the bi-plane square grid. The effect of the disturbance on the velocity statistics is discussed.

2. Analytical methods

2.1 VITA technique

The VITA (Variable Interval Time Average) technique (Blackwelder & Kaplan 1976, Blackwelder & Haritonidis 1983, Chen & Blackwelder 1978, Osaka et al. 1986) is one of the conditional mean methods used to detect coherent motions in turbulent flows. The VITA technique is appropriate for detecting the bursting events in a TBL since the bursting events accompany the large velocity fluctuations. Following the general VITA technique (Blackwelder & Haritonidis 1983), we define the variable-interval time average of the fluctuating streamwise velocity $\tilde{u}$ as

$$v_a(t;x,T)=\frac{1}{T}\int_{t-T/2}^{t+T/2}\tilde{u}(t')^2\,dt'-\left[\frac{1}{T}\int_{t-T/2}^{t+T/2}\tilde{u}(t')\,dt'\right]^2 \tag{1}$$

where T is the averaging time. Note that v_a approaches the conventional time-averaged result as T increases. The detection criterion is established by introducing a threshold value for the VITA variance signal. Thus, the detection function $\alpha_u(t)$ is defined as (Blackwelder & Haritonidis 1983, Chen & Blackwelder 1978, Osaka et al. 1986)

$$\alpha_u(t)=\begin{cases}1;\ v_a(t)\geq Ku_{rms}^2 \text{ and } \dfrac{d}{dt}\left[\tilde{u}(t)-\bar{u}\right]>0\\ 0;\ \text{otherwise,}\end{cases} \tag{2}$$

where $\bar{u}$ is the time-averaged mean velocity, u_{rms} is the rms (root mean square) value of velocity fluctuations, and K is the threshold value, which is constant. In general, the selection of K and T is important for detecting the bursting events using the VITA technique. In this study, we chose $K=1$ and $T^+=Tu_\tau^2/\nu=20$, on the basis of a previous study (Osaka et al. 1986), where u_τ is the friction velocity and ν is the kinematic viscosity. We have carefully verified that the detected burst frequency is in a good agreement with previously published data (Blackwelder & Haritonidis 1983, Osaka et al. 1986).

2.2 Methods for detecting large-scale coherent motions

The large-scale coherent motions in the outer turbulent/nonturbulent interface of the TBL are detected using the following method. The first probe from the top of the rake, which is placed near the turbulent/nonturbulent interface of the TBL ($y/\delta=1.23$; y and δ are the distance from the wall and the thickness of the boundary layer, respectively), is used to detect the large-scale coherent motions since these motions pass through this probe. The detection of the motions depends on both u and $\partial u/\partial t$ at $y/\delta=1.23$. Note that the direction of the rotation is based on the configuration shown in Figs. 1 and 2; the flow is from the left to the right along the x-direction. Therefore, the mean spanwise vorticity is in the clockwise direction.

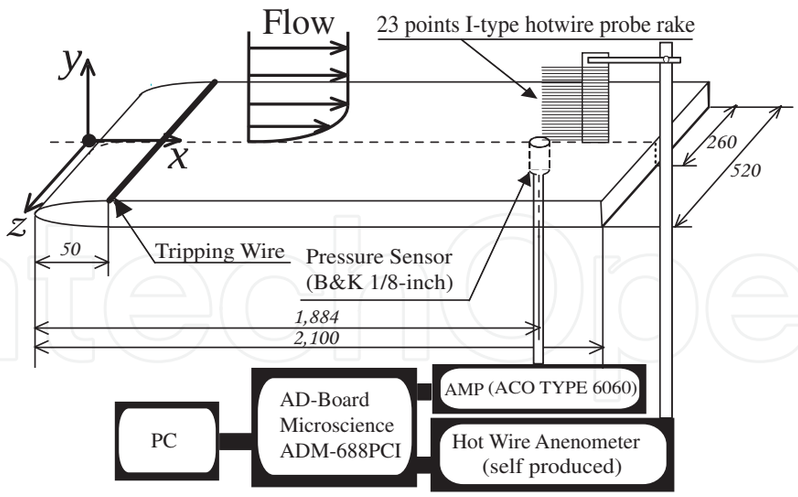

Fig. 1. Experimental setup

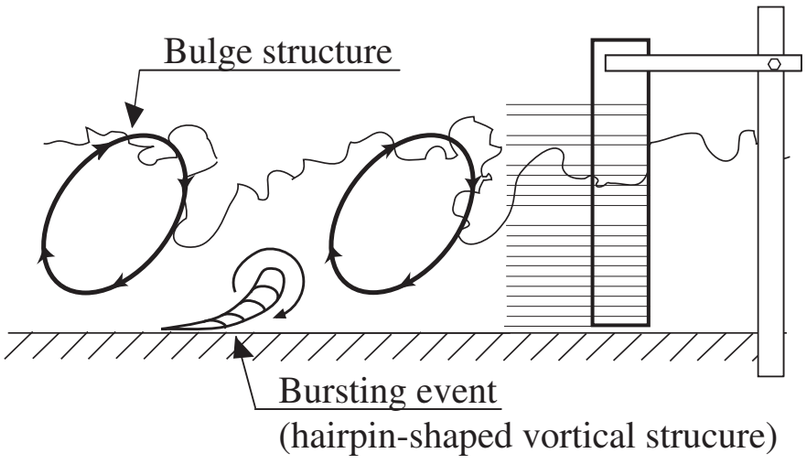

Fig. 2. Schematic of bulge structure and bursting event (not to scale)

2.2.1 Detection of clockwise large-scale coherent motions

The large velocity fluctuation at $y/\delta = 1.23$ with *acceleration* is associated with the `bulge' structure, which is the large-scale (δ-scale) vortical structure rotating in the same direction as the mean vorticity (i.e. in the clockwise direction). Therefore, we detect the bulge structure by using the following conditions:

$$\left[\tilde{u}(t) - \overline{u}\right]^2 \geq K' u_{rms}^2 \quad \text{and} \quad \frac{d}{dt}\left[\tilde{u}(t) - \overline{u}\right] > 0 \tag{3}$$

where K' is the threshold value, which is constant. In this study, from a careful inspection of the detected signals, K' has been chosen equal to 3.

2.2.2 Detection of anticlockwise large-scale coherent motions

The large velocity fluctuation at $y/\delta = 1.23$ with *deceleration* is associated with the `valley' structure, which is the large-scale (δ-scale) structure at the edge of the bulges (Robinson

1991) rotating in the opposite direction of the mean vorticity (i.e. in the anticlockwise direction). Therefore, we detect the valley structure by using the following conditions:

$$\left[\tilde{u}(t)-\overline{u}\right]^2 \geq K' u_{rms}^2 \quad \text{and} \quad \frac{d}{dt}\left[\tilde{u}(t)-\overline{u}\right] < 0 \tag{4}$$

It has been verified that the value of $K'=3$ is appropriate for detecting the valley structures.

2.3 KL expansion

The KL（Karhunen-Loéve）expansion, which is also known as the proper orthogonal decomposition (POD) method and is an extension of the general Fourier series (Davenport & Root 1958, Lumley 1967, 1981), is the representation of a stochastic process as a linear combination of orthogonal functions. The basis functions of the expansion are defined such that the coefficients are uncorrelated (independent) with each other and are arranged in the descending order according to the magnitude of their eigenvalues. The sum of all the eigenvalues corresponds to the sum of the mean square values in the entire region where the KL expansion is applied. Here, the KL expansion is applied for the simultaneous measurement of the streamwise velocities at 23 points in the TBL. Therefore, there are 23 modes ($n=1\sim 23$) in the KL expansion. The lower modes are expected to extract the turbulence structures in the near-wall region (i.e., the inner region), where turbulence energy is larger, and the higher modes are expected to extract the turbulence structures from the outer region to the outside of boundary layer, where turbulence energy is smaller. In this study, the sum of the first three modes (lower modes) retains 65% of the total energy; therefore, the flow field reconstructed by using the lower modes ($n=1\sim 3$) is considered to represent the energetic coherent motions. The modes from 4 to 23, which contain the rest of the 35% energy, are regarded as the higher modes in this work.

3. Experiments

3.1 Experimental apparatus

Experiments are carried out in an Eiffel-type wind tunnel. The length, height, and span of the test section of this tunnel are 2,600, 300, and 520 mm, respectively. The TBL is developed along a smooth flat plate (Fig. 1) placed horizontally in the wind tunnel. The plate is 2,100 mm in length, 8 mm in thickness, and 520 mm in span and is made of Bakelite in order to reduce the heat loss from the hot-wire probe in near-wall measurements. The leading edge of the plate has a parabolic shape. To generate a fully developed TBL in a short distance from the leading edge, transition was promoted by using a tripping wire of 1.0 mm diameter placed 50 mm downstream from the leading edge of the plate, as shown in Fig. 1. The zero-pressure-gradient condition is achieved by adjusting the height of the test section. The coordinate system is as follows: the *x*-axis is along the streamwise direction starting from the leading edge, the *y*-axis is in the vertical direction, and the *z*-axis is along the spanwise direction (see Fig. 1).

3.2 Velocity and wall static pressure measurements

A constant-temperature hot-wire anemometer (CTA) is used for the velocity measurement. The rake consists of 23 I-type probes, which covers the entire TBL at $x=1{,}884$ mm; the sensors of the rake cover a length of $y=0.1\sim 48.5$ mm. The wires are made of tungsten. The length of the sensor is $l=1$ mm and its diameter is $d=5$ μm, giving an aspect ratio of

$l/d = 200$. By comparing the data obtained from a single I-type probe with those from the rake of I-type probes, it has been confirmed that there is no interference between the probes, which are placed with 2.2 mm apart from each other.

To measure the instantaneous static pressure at the wall, the 1/8 inch microphone pressure sensor (Brüel & Kjær Type 4138) is used. The sensor is mounted flush to the wall surface at the measurement position ($x = 1{,}884$ mm) through a pressure hole of $D = 0.6$ mm diameter. The frequency response of the pressure sensor has been checked; both the phase difference φ and the magnitude ratio M between the input signal and the output signal from the sensor exhibit flat responses up to 7 kHz. These results suggest that the frequency response limit of the pressure sensor is 7 kHz. Note that nondimensional diameter of the sensing area in this study is $D^+ = Du_\tau / \nu = 18$. Previous studies (Gravante et al. 1998, Schewe 1983) have shown that when $D^+ < 19 \sim 20$, the spatial resolution is sufficient to resolve the essential structures of the static pressure fluctuations at the wall. Therefore, in addition to the frequency response, the spatial resolution is sufficient to measure the static pressure fluctuations at the wall. In fact, we have confirmed that when $D^+ < 18$, the power spectra of wall static pressure fluctuations are identical.

3.3 Experimental conditions and data sampling method

The mean speed of the uniform flow is set at $U_0 = 10.9$ m/s. The unit Reynolds number is $\mathrm{Re} = U_0 / \nu = 7.38 \times 10^5$ m^{-1}, and the Reynolds number based on the momentum thickness at the measurement point ($x = 1{,}884$ mm) is $\mathrm{Re}_\theta = 2{,}820$. Note that the spatial resolution of the hot-wire probe in the near-wall measurement is sufficient for $\mathrm{Re}_\theta < 5{,}000$ (Robinson 1991). The δ and u_τ at the measurement point ($x = 1{,}884$ mm) are 41 mm and 0.453 m/s, respectively. We have confirmed that there is no pressure gradient in the streamwise direction, and the mean flow is two-dimensional. The sampling frequency and sample size are 10 kHz and 229,376, respectively, and are sufficient to obtain reliable statistics: these parameters are based on the performance of the A/D converter (Microscience ADM-688PCI) and the computer (Dell Dimension 8200) used. The output voltage signals from the hot-wire anemometer and the pressure sensor are converted into 12-bit digital data by the A/D converter and recorded on the hard disc of the computer. The A/D converter and the digital output board are PCI interface boards and are synchronized through master-slave connections. The time lag between the output of the clock signal from the master unit and the input of the signal into the slave unit is only 125 ns; therefore, very fast multichannel sampling is achieved. To confirm this point, we input the same wave pattern generated by the function generator into the whole channels simultaneously, and compare the output signals. The result showed that the output signals are the same and no discernible time lag is observed. Statistical processing of the digitized data was carried out using the computer.

4. Results and discussion

4.1 Reliability of measurements

The vertical profile of streamwise mean velocity is shown in Fig. 3, where $U^+ = U/u_\tau$ and $y^+ = yu_\tau/\nu$. The log-law region can be seen for $30 < y^+ < 200$. Figures 4 and 5 show the power spectrum of streamwise velocity fluctuations normalized by the squared rms value of

the velocity fluctuations, u_{rms}^2, and the power spectrum of the wall static pressure fluctuations normalized by the squared rms value of the wall static pressure fluctuations, p_{rms}^2, respectively. Figure 4 shows that the power spectrum of the longitudinal velocity fluctuations collapses irrespective of y^+. The spectrum also shows the -1 and -5/3 decay regions (Perry et al. 1986). On the other hand, the power spectrum of wall static pressure fluctuations (Fig. 5) has the -1, -7/3, and -5 decay regions, and the result agrees with that of previous experiments carried out by Gravante et al. (1998) and Löfdahl (1996). In addition, turbulence intensities and probability density functions (not shown) are in good agreement with those found in previous studies. Therefore, it is confirmed that the present measurements of velocity and wall static pressure fluctuations are highly accurate.

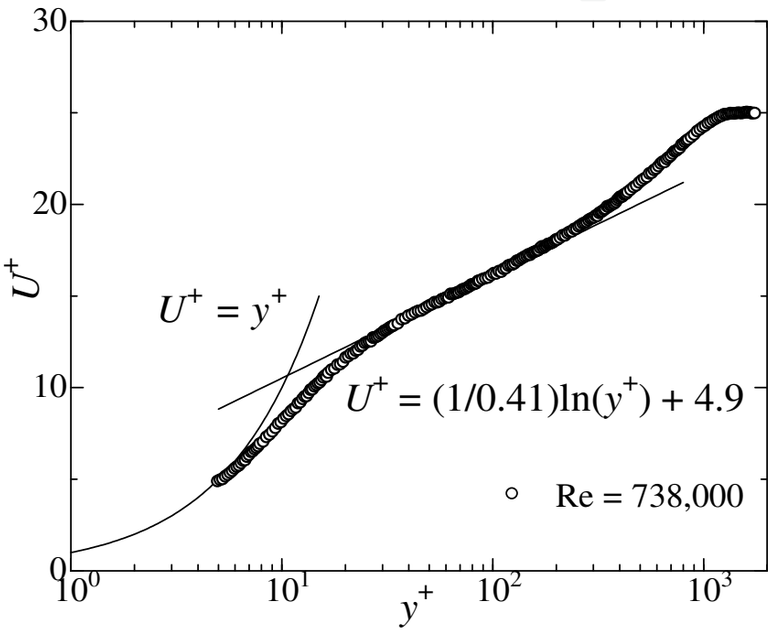

Fig. 3. Vertical profile of streamwise mean velocity

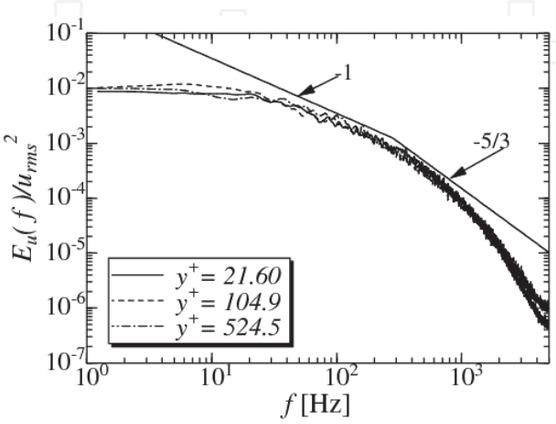

Fig. 4. Power spectrum of streamwise velocity fluctuations

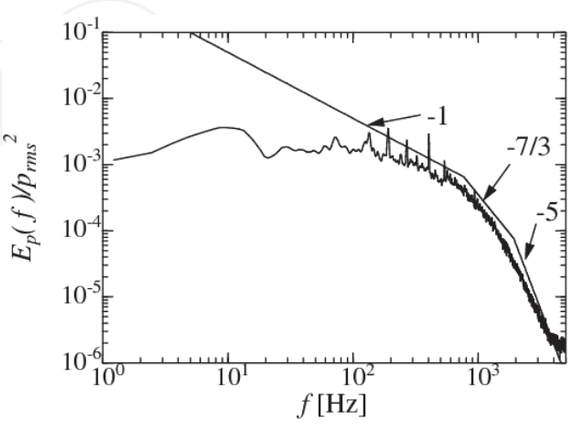

Fig. 5. Power spectrum of wall static pressure fluctuations

4.2 Relationships between bursting events and large-scale coherent motions

The clockwise and anticlockwise large-scale coherent motions are detected using the method proposed in the subsection 2.2, and the results are shown in Figs. 6 and 7, respectively. In Figs. 6 and 7, the upper and lower graphs show the conditionally averaged time histories of the normalized velocity, $\langle \tilde{u}(\tau) \rangle' = \left(\langle \tilde{u}(\tau) \rangle - \overline{u} \right) / u_{rms}$, and the conditionally averaged time histories of normalized wall static pressure, $\langle \tilde{p}(\tau) \rangle' = \left(\langle \tilde{p}(\tau) \rangle - \overline{p} \right) / p_{rms}$, respectively. Here, $\langle \tilde{u}(\tau) \rangle$ and $\langle \tilde{p}(\tau) \rangle$ are the ensemble-averaged values of conditionally sampled velocity and wall static pressure, respectively, and $\overline{u}$ and $\overline{p}$ are the ordinary (non-conditional) time-averaged velocity and wall static pressure, respectively. In Figs. 6 and 7, τ is the time lag from the detection time at which the instantaneous velocity signal takes the maximum or minimum value at the detection point of $y/\delta = 1.23$, and is normalized by using U_0 and δ. Figure 6 shows that when the clockwise large-scale coherent motion passes, the velocity increases outside the TBL ($y/\delta > 1$) and decreases inside the TBL ($y/\delta < 1$). The result suggests the presence of a rotational flow whose center is located near the turbulent/nonturbulent interface: this structure corresponds to the bulge (Kobashi et al. 1984). It is also observed from Fig. 6 that the wall static pressure decreases when the clockwise large-scale coherent motion passes. It is presumed that measured decrease in the wall static pressure is associated with the low pressure in the clockwise large-scale coherent motion (Robinson 1991).

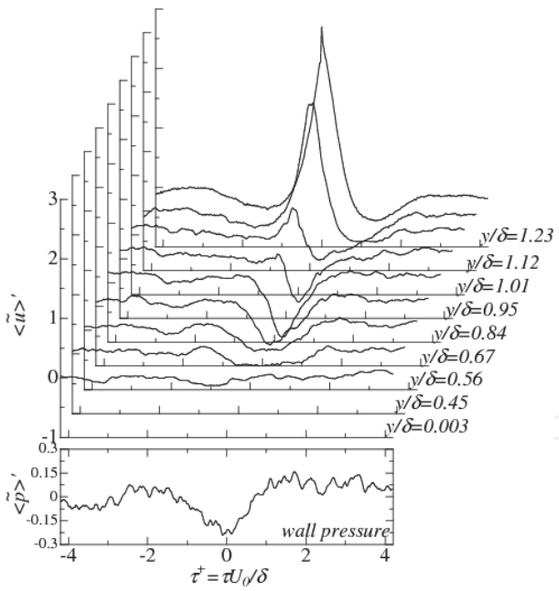

Fig. 6. Ensemble-averaged time histories of conditionally sampled velocity and wall static pressure corresponding to the bulge structure

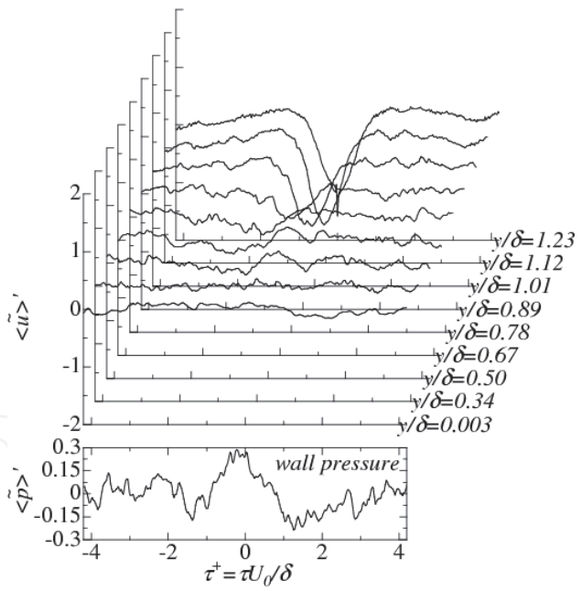

Fig. 7. Ensemble-averaged time histories of conditionally sampled velocity and wall static pressure corresponding to the valley structure

On the other hand, Fig. 7 shows that when the anticlockwise large-scale coherent motion passes, the velocity decreases outside the TBL ($y/\delta > 1$) and slightly increases inside the TBL ($y/\delta < 1$). The detected signals suggest the valley, which exists at the edge of the bulges. It

has been reported (Robinson 1991, Thomas & Bull 1983) that there is an inflow from the free-stream flow into the turbulent region, and the inflow has an instantaneous velocity vector that is against the mean flow. Therefore, it is expected that the decrease in the velocity in the outer region in Fig. 7 is associated with the inflow from the free-stream flow. The wall static pressure increases when the anticlockwise large-scale coherent motion passes. These results are in agreement with the model for the structure of a TBL proposed by Thomas & Bull (1983).

The VITA technique is applied to the raw signals to detect the bursting events. Figure 8 shows the ensemble-averaged time histories of conditionally sampled velocity

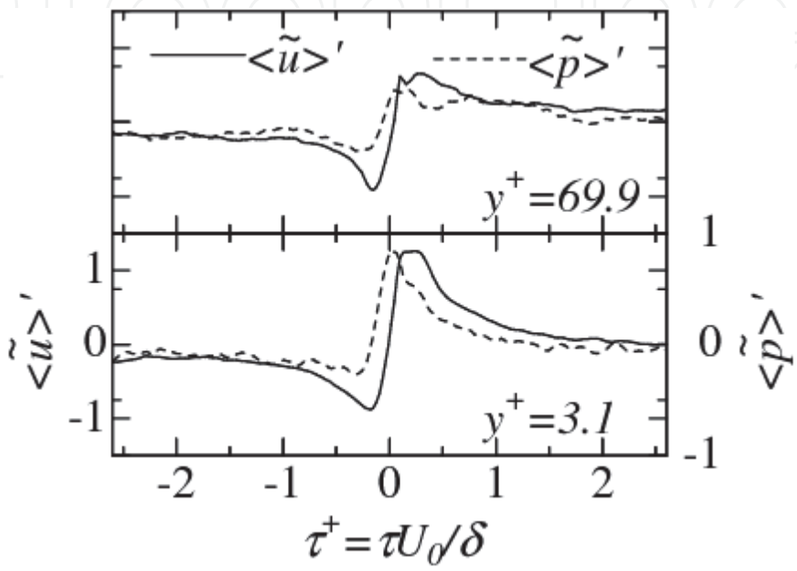

Fig. 8. Ensemble-averaged time histories of conditionally sampled velocity and wall static pressure. The detection is based on the VITA technique

$\left\langle \tilde{u}(\tau) \right\rangle' = \left(\left\langle \tilde{u}(\tau) \right\rangle - \bar{u} \right) / u_{rms}$ and of conditionally sampled wall static pressure $\left\langle \tilde{p}(\tau) \right\rangle' = \left(\left\langle \tilde{p}(\tau) \right\rangle - \bar{p} \right) / p_{rms}$. Here, $\left\langle \tilde{u}(\tau) \right\rangle$ and $\left\langle \tilde{p}(\tau) \right\rangle$ are the conditionally averaged velocity and wall static pressure by the VITA technique, respectively. The solid and broken lines in Fig. 8 denote $\left\langle \tilde{u}(\tau) \right\rangle'$ and $\left\langle \tilde{p}(\tau) \right\rangle'$, respectively. τ is the time lag from the detection time at which the instantaneous velocity $\tilde{u}(t)$ is the same as the ordinary (non-conditional) time-averaged velocity $\bar{u}$ at each measuring point. Figure 8 shows the cycle of events of ejection ($\left\langle \tilde{u}(\tau) \right\rangle' < 0$) at $\tau < 0$, which is the upward motion of a low-speed fluid lump, and sweep ($\left\langle \tilde{u}(\tau) \right\rangle' > 0$) at $\tau > 0$, which is the downward motion of a high-speed fluid lump (Osaka et al. 1986). The wall static pressure exhibits a rapid increase when the burst occurs above the measurement point (Kobashi et al. 1984). Considering the results shown in Figs. 6 and 7 together with the result in Fig. 8, it is concluded that the bulge structure, which is accompanied by the pressure decrease, cannot coexist with the bursting event, which is accompanied by the pressure increase. On the other hand, the valley structure, which is accompanied by the pressure increase, can coexist with the bursting event.

4.3 Flow field reconstructed by using lower modes (*n*=1 ~ 3)

Using the method proposed in the subsection 2.2, the clockwise and anticlockwise large-scale coherent motions are detected in the flow field reconstructed by using the lower

modes ($n=1\sim3$) of the KL expansion, and the results are shown in Figs. 9 and 10, respectively. Figures 9 and 10 show that both the clockwise large-scale coherent motion (i.e. bulge), which is accompanied by the pressure decrease, and the anticlockwise large-scale coherent motion (i.e. valley), which is accompanied by the pressure increase, exist in

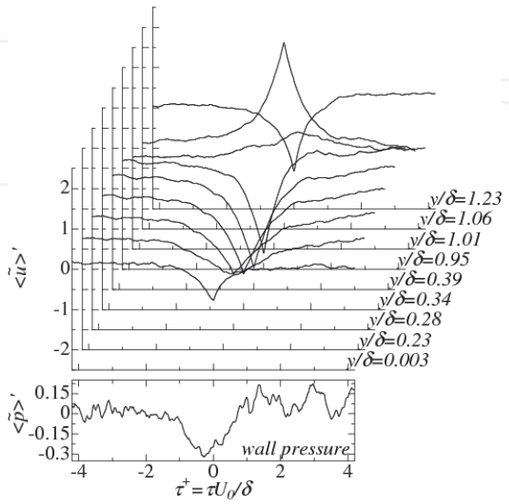

Fig. 9. Ensemble-averaged time histories of conditionally sampled velocity and wall static pressure when the velocity is reconstructed by the lower modes ($n=1\sim3$) and the detection method of the clockwise bulge structure is applied.

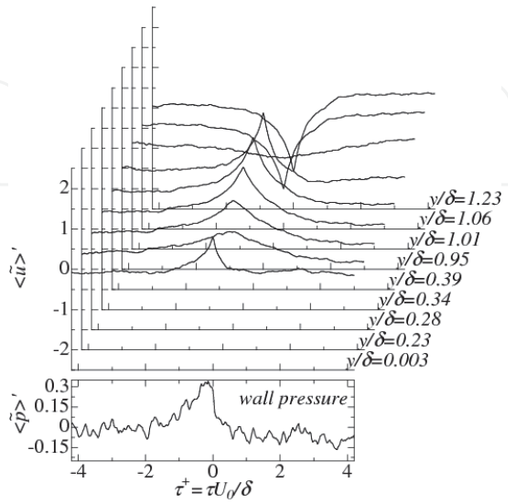

Fig. 10. Ensemble-averaged time histories of conditionally sampled velocity and wall static pressure when the velocity is reconstructed by the lower modes ($n=1\sim3$) and the detection method of the anticlockwise valley structure is applied.

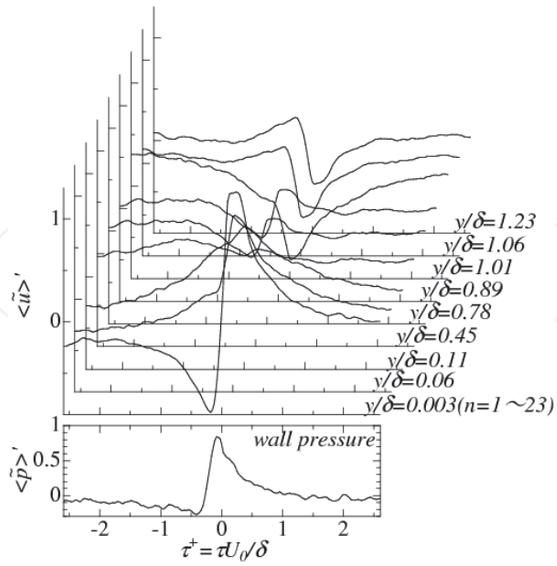

Fig. 11. Ensemble-averaged time histories of conditionally sampled velocity and wall static pressure when the velocity is reconstructed by the lower modes ($n=1\sim3$). The detection is based on the VITA technique applied to the original flow field ($n=1\sim23$) at $y/\delta=0.003$

the flow field reconstructed by using the lower modes. Comparing these results with those shown in Figs. 6 and 7, which are obtained by applying the method to the original flow field ($n = 1 \sim 23$), it is found that these structures are more clearly observed in the flow field reconstructed by using the lower modes and they are observed even near the wall.

Figure 11 shows the ensemble-averaged time histories of conditionally sampled velocity and wall static pressure when the velocity is reconstructed by the lower modes ($n = 1 \sim 3$) and the detection by the VITA technique is applied to the original flow field ($n = 1 \sim 23$) at $y/\delta = 0.003$. It is observed from Fig. 11 that the velocity inside the TBL (in the reconstructed flow) increases and the velocity outside the TBL (in the reconstructed flow) decreases when the bursting event occurs. These velocity patterns are similar to those during the anticlockwise large-scale coherent motion (i.e. valley). Thus, the results suggest that the bursting event and valley can coexist at the same longitudinal location in the flow reconstructed by using the lower modes ($n = 1 \sim 3$).

4.4 Flow field reconstructed by using higher modes (*n*=4 ~ 23)

Using the method proposed in the subsection 2.2, the clockwise and anticlockwise large-scale coherent motions are detected in the flow field reconstructed by using the higher modes ($n = 4 \sim 23$) of the KL expansion, and the results are shown in Figs. 12 and 13, respectively. Figure 12 (for the bulge) shows a velocity variation near the wall. However, the velocity hardly changes near the wall in Fig. 13 (for the valley). These results suggest that in the flow field reconstructed by using the higher modes, only the clockwise large-scale

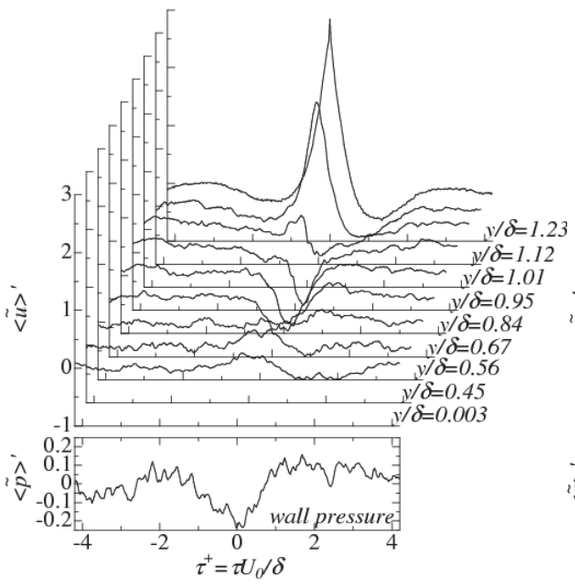

Fig. 12. Ensemble-averaged time histories of conditionally sampled velocity and wall static pressure when the velocity is reconstructed by the higher modes ($n = 4 \sim 23$) and the detection method of the clockwise bulge structure is applied.

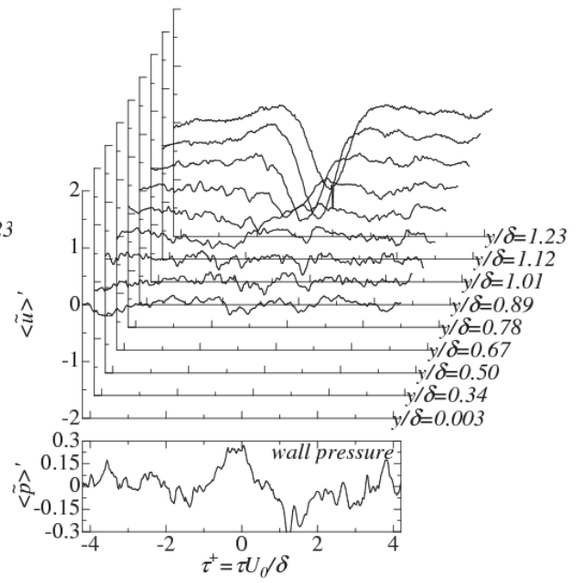

Fig. 13. Ensemble-averaged time histories of conditionally sampled velocity and wall static pressure when the velocity is reconstructed by the higher modes ($n = 4 \sim 23$) and the detection method of the anticlockwise valley structure is applied.

coherent motion (i.e. bulge) exists near the wall and the anticlockwise large-scale coherent motion (i.e. valley) does not influence the flow field near the wall. These results also suggest that the turbulent kinetic energy in the bulge structure is larger than that in the valley structure. This result is consistent with the fact that the valley is generated by the bulge structures.
Figure 14 shows the ensemble-averaged time histories of conditionally sampled velocity and wall static pressure when the velocity is reconstructed by the higher modes ($n = 4 \sim 23$) and the detection by the VITA technique is applied to the original flow field ($n = 1 \sim 23$) at $y / \delta = 0.003$. Figure 14 shows that when the bursting events are detected, the velocity in the outer region does not change in the reconstructed flow. This result suggests that in the flow field reconstructed by using the higher modes, the large-scale coherent motions are weakly associated with the bursting events.

4.5 Effect of freestream turbulence on the Turbulent Boundary Layer

In the industrial flows such as those in turbomachines and heat exchangers, inflow streams often contain the turbulent eddies generated by the upstream structures. These free stream turbulence influences the large scale coherent structure and the turbulence characteristics of the TBL. In this subsection, some experimental data on the statistical properties of TBL affected by the freestream turbulence generated by the square grid are demonstrated.
The experiments are performed by using the experimental apparatus shown in the subsection 3.1. The turbulence-generating grid is installed at 100mm upstream from the leading edge of the plate. The square-mesh biplane grid *M*10 is used. *M*10 was constructed from square-sectioned aluminium rods. The mesh size M and the rod thickness d are 3×10^{-2}m and 6×10^{-3}m, respectively, and therefore, its solidity is $\sigma = 0.36$. The mean speed of free stream flow when the grid is installed is set at $U_0 = 10.1$m/s. The unit Reynolds number is $\mathrm{Re} = U_0/\nu = 6.84 \times10^5\mathrm{m}^{-1}$ and the Reynolds number based on the momentum thickness at the measurement point (x=1,880 mm) is $\mathrm{Re}_\theta = 3{,}000$. When the grid is not installed, the flow condition is adjusted to realize $\mathrm{Re}_\theta = 3{,}000$ at the same measurement point (x=1,880 mm). The instantaneous streamwise velocity is measured by the hot-wire CTA with the I-type probe. The wire is made of tungsten. The length of sensor is 1.0 mm and its diameter is 5μm, giving an aspect ratio of $l/d = 200$. The output signals from the CTA are digitized and recorded on the hard disc using the data recording unit (KEYENCE WR-60). The sampling frequency and sample size are 20 kHz and 524,288(=2^{19}), respectively.
The vertical profiles of $y^+ \, dU^+/dy^+$ in both cases with and without the grid are shown in Fig.15, where the result by the Direct Numerical Simulation (DNS) in the case of $\mathrm{Re}_\theta = 1{,}410$ (Spalart 1988) is also depicted for the comparison. Note that in the logarithmic region the value of $y^+ \, dU^+/dy^+$ should be constant, i.e., $y^+ \, dU^+/dy^+ = 1/\kappa$. From Fig.15, it is found that the logarithmic region for the case with the grid expands to the outer side of the TBL in comparison with the case without the grid. Figure 16 shows the vertical profiles of the velocity fluctuation rms value u_{rms} normalized by the friction velocity u_τ, i.e., $u^+_{rms} = u_{rms} / u_\tau$. It is found that u^+_{rms} in the case with the grid increases in comparison with the case without the grid. However it should be noted that in general the free-stream disturbance does not always increase u^+_{rms} , and in some cases u^+_{rms} decreases (Hancock & Bradshow 1989, Nagata et al. 2011). The effects of free-stream disturbance on the characteristics of the TBL are still open question. The future works are expected to elucidate the relation between the free-stream disturbance and the flow dynamics of the TBL.

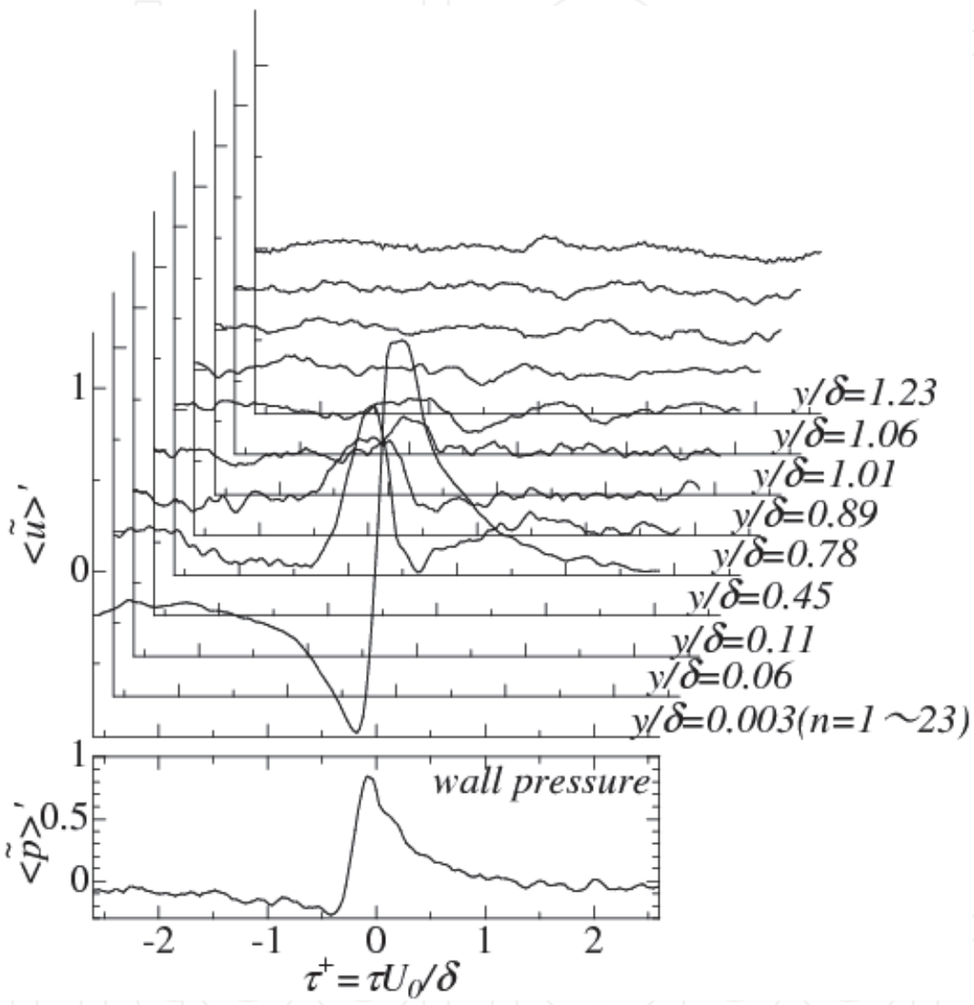

Fig. 14. Ensemble-averaged time histories of conditionally sampled velocity and wall static pressure when the velocity is reconstructed by the higher modes ($n = 4 \sim 23$). The detection is based on the VITA technique applied to the original flow field ($n = 1 \sim 23$) at $y / \delta = 0.003$

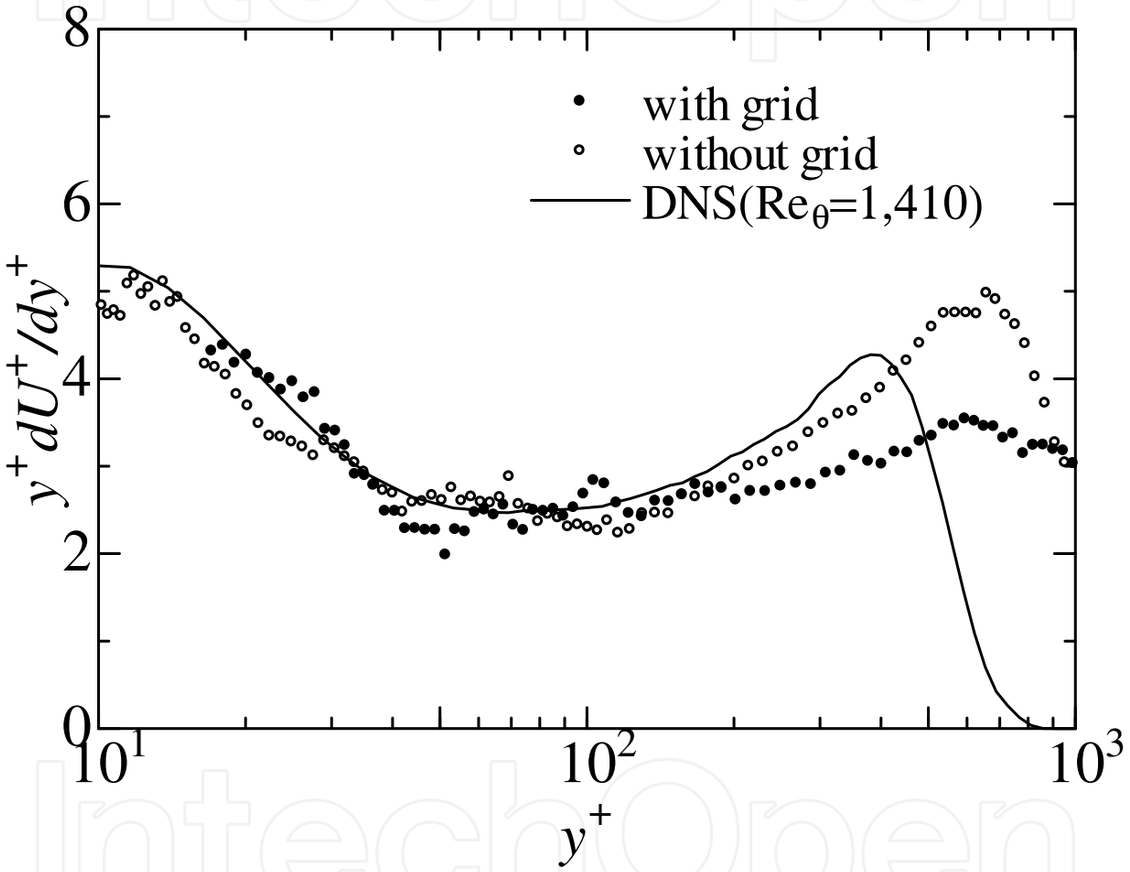

Fig. 15. The vertical profiles of $y^+ dU^+/dy^+$

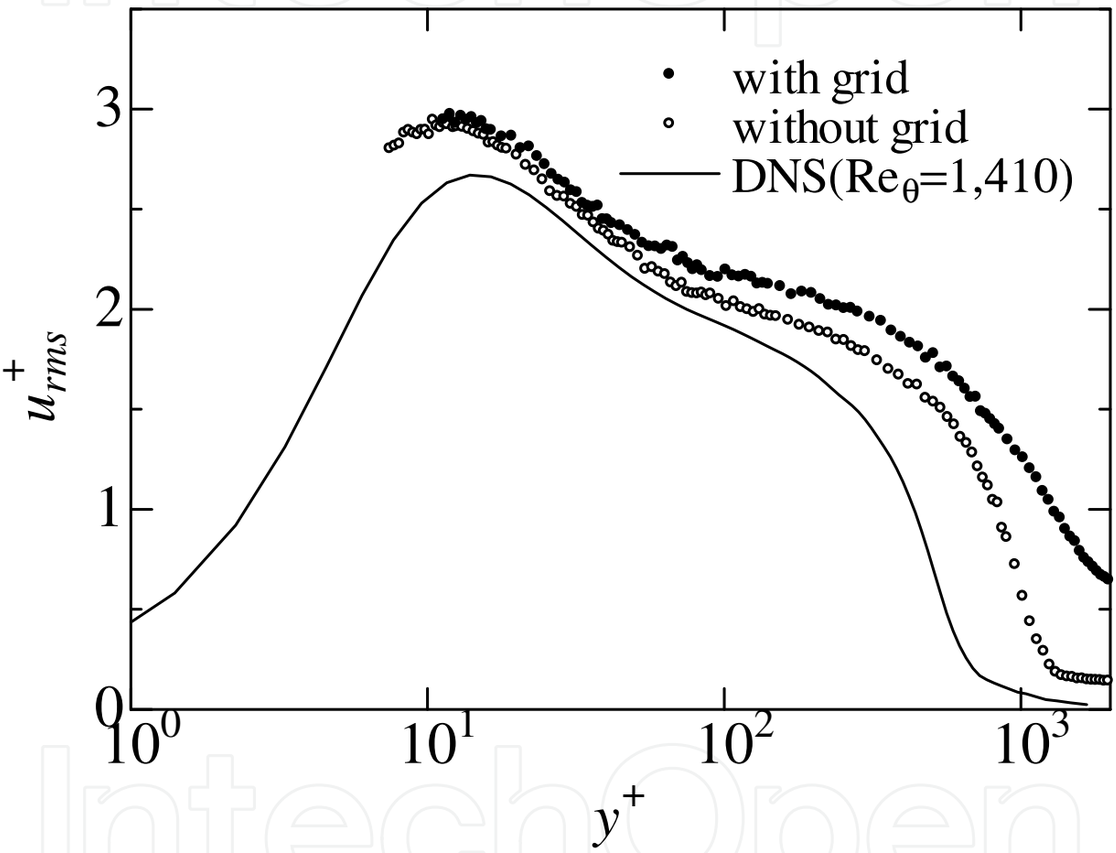

Fig. 16. The vertical profiles of u^+_{rms}

5. Conclusions

Multipoint instantaneous streamwise velocities and instantaneous wall static pressures have been simultaneously measured by using a combination of a rake consisting of 23 I-type hot-wire probes and a microphone pressure sensor in a fully developed, zero-pressure-gradient turbulent boundary layer (TBL) in a wind tunnel. The KL（Karhunen-Loéve）expansion, the VITA technique and the newly proposed method for the detection of large-scale coherent motions were applied to examine the relationships between large-scale coherent motions and the bursting events. Further, the statistical properties of the TBL affected by the freestream turbulence generated by the square grid were investigated.
The main results obtained in this chapter are summarized as follows:

1. The structure of the TBL inferred from the present experiment is in agreement with the TBL model proposed by Thomas & Bull (1983).
2. The bursting events and valley structure (both accompanied by an increase in wall static pressure) can coexist at the same longitudinal location, whereas the bursting events and bulge structure cannot coexist with each other.
3. In the flow field reconstructed by using the lower modes, both the bulge structure, which is accompanied by bursting events, and the valley structure, which is not accompanied by the bursting events, exist. On the other hand, in the flow field reconstructed by using the higher modes, the large-scale coherent structures are weakly associated with the bursting events.
4. The grid turbulence introduced into the outer mainstream has the effect to enlarge the logarithmic region to the outer side of turbulent boundary layer.

6. Acknowledgment

This study was partially supported by the Japanese Ministry of Education, Culture, Sports, Science and Technology through Grants-in-Aid (Nos. 22360076 and 22360077).

7. References

Blackwelder, R. F. & Kaplan, R. E. (1976). On the Wall Structure of the Turbulent Boundary Layer. *Journal of Fluid Mechanics,* Vol.76, pp.89-112

Blackwelder, R. F. & Haritonidis, J. H. (1983). Scaling of the Bursting Frequency in Turbulent Boundary Layers. *Journal of Fluid Mechanics,* Vol.132, pp.87-103

Blair, M. F. (1983). Influence of free-stream turbulence on turbulent boundary layer heat transfer and mean profile. Part 1 – Experimental Data. *Transactions of the ASME: Journal of Heat Transfer*, Vol.15, pp.33-40

Chen, C-H. P. & Blackwelder, R. F. (1978). Large-scale Motion in a Turbulent Boundary Layer: A Study Using Temperature Contamination. *Journal of Fluid Mechanics,* Vol.89, pp.1-31

Gravante, S. P.; Naguib, A. M.; Wark, C. E. & Nagib, H. M. (1998). Characterization of the Pressure Fluctuations Under a Fully Developed Turbulent Boundary Layer. *AIAA Journal*, Vol. 36, No. 10, pp.1808-1816

Davenport, W. B. Jr. & Root, W. L. (1958). *An Introduction to the Theory of Random Signals and Noise*, pp.96-101, McGraw-Hill

Hancock, P.E. & Bradshaw, P. (1989). Turbulence Structure of a Boundary Layer Beneath a Turbulent Free Stream. *Journal of Fluid Mechanics*, Vol.205, pp.45-76

Hoffman, J. A. (1981). Effects of free-stream turbulence on diffuser performance, *Transactions of the ASME: Journal of Fluids Engineering*, Vol.103, pp.385-390

Ichijo, M. & Kobashi, Y. (1982). The Turbulence Structure and Wall Pressure Fluctuations of a Boundary Layer. *Nagare,* Vol.1, pp. 350-359

Kobashi, Y.; Komoda, H. & Ichijo, M. (1984). Wall Pressure Fluctuation and the Turbulent Structure of a Boundary Layer. In: *Turbulence and Chaotic Phenomena in Fluids*, ed. Tatsumi, T., pp.461-466, Elsevier

Löfdahl, L. (1996). Small Silicon Pressure Transducers for Space-Time Correlation Measurements in a Flat Plate Boundary Layer. *Transactions of ASME: Journal of Fluids Engineering*, Vol.118 , pp.457-463

Lumley, J. L. (1967). The Structure of Inhomogeneous Turbulent Flows. In: *Atmospheric Turbulence and Radio Wave Propagation*, eds. Yaglom, A. M. and Tararsky, V. I., pp.166-178. Nauka, Moscow

Lumley, J. L. (1981). In: *Transition and Turbulence*, ed. Meyer, R. E., pp.215-241. Academic, New York

McDonald, H. & Fish, R.W. (1973). Practical Calculations of Transitional Boundary Layers. *International Journal of Heat and Mass Transfer*, Vol.16, pp.1729-1744

Nagata, K.; Sakai, Y. & Komori, S. (2011). Effects of Small-Scale Freestream Turbulence on Turbulent Boundary Layers with and without Thermal convection. *Physics of Fluids,* in press

Osaka, H.; Mochizuki, S. & Nishi, S. (1986). On the Detection of the Bursting Events with the VITA Technique. *Transactions of the Japan Society of Mechanical Engineers, Series B* (in Japanese). Vol.52, No.481, pp.3224-3229

Perry, A. E.; Henbest, S. & Chong, M. S. (1986). A Theoretical and Experimental Study of Wall Turbulence. *Journal of Fluid Mechanics*, Vol.165, pp.163-199

Robinson, S. K. (1991). Coherent Motions in the Turbulent Boundary Layer. *Annual Review of Fluid Mechanics,* Vol.23, pp. 601-639

Schewe, G. (1983). On the Structure and Resolution of Wall-pressure Fluctuations Associated with Turbulent Boundary-layer Flow. *Journal of Fluid Mechanics*, Vol.134, pp.311-328

Spalart, P. R. (1988). Direct Simulation of a Turbulent Boundary Layer up to $R_\theta = 1410$. *Journal of Fluid Mechanics*, Vol.187, pp.61-98

Thomas, A. S. W. & Bull, M. K. (1983). On the Role of Wall-pressure Fluctuations in Deterministic Motions in the Turbulent Boundary Layer. *Journal of Fluid Mechanics*, Vol.128, pp.283-322

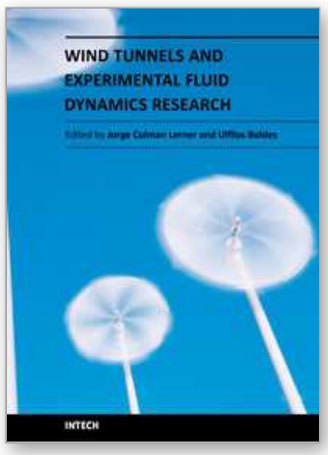

Wind Tunnels and Experimental Fluid Dynamics Research

Edited by Prof. Jorge Colman Lerner

ISBN 978-953-307-623-2
Hard cover, 709 pages
Publisher InTech
Published online 27, July, 2011
Published in print edition July, 2011

The book â€œWind Tunnels and Experimental Fluid Dynamics Researchâ€ is comprised of 33 chapters divided in five sections. The first 12 chapters discuss wind tunnel facilities and experiments in incompressible flow, while the next seven chapters deal with building dynamics, flow control and fluid mechanics. Third section of the book is dedicated to chapters discussing aerodynamic field measurements and real full scale analysis (chapters 20-22). Chapters in the last two sections deal with turbulent structure analysis (chapters 23-25) and wind tunnels in compressible flow (chapters 26-33). Contributions from a large number of international experts make this publication a highly valuable resource in wind tunnels and fluid dynamics field of research.

How to reference

In order to correctly reference this scholarly work, feel free to copy and paste the following:

Yasuhiko Sakai, Kouji Nagata and Hiroki Suzuki (2011). Relationships between Large-Scale Coherent Motions and Bursting Events in a Turbulent Boundary Layer, Wind Tunnels and Experimental Fluid Dynamics Research, Prof. Jorge Colman Lerner (Ed.), ISBN: 978-953-307-623-2, InTech, Available from: http://www.intechopen.com/books/wind-tunnels-and-experimental-fluid-dynamics-research/relationships-between-large-scale-coherent-motions-and-bursting-events-in-a-turbulent-boundary-layer

INTECH
open science | open minds

InTech Europe
University Campus STeP Ri
Slavka Krautzeka 83/A
51000 Rijeka, Croatia
Phone: +385 (51) 770 447
Fax: +385 (51) 686 166
www.intechopen.com

InTech China
Unit 405, Office Block, Hotel Equatorial Shanghai
No.65, Yan An Road (West), Shanghai, 200040, China
中国上海市延安西路65号上海国际贵都大饭店办公楼405单元
Phone: +86-21-62489820
Fax: +86-21-62489821

IntechOpen